ENVIRONMENTAL RESEARCH

LETTERS

LETTER • OPEN ACCESS

Expanding infrastructure and growing anthropogenic impacts along Arctic coasts

To cite this article: Annett Bartsch et al 2021 Environ. Res. Lett. 16 115013

View the <u>article online</u> for updates and enhancements.

You may also like

- Human impact parameterizations in global hydrological models improve estimates of monthly discharges and hydrological extremes: a multi-model validation study T I E Veldkamp, F Zhao, P J Ward et al.
- <u>Human impact on wildfires varies between</u> regions and with vegetation productivity
 Gitta Lasslop and Silvia Kloster
- Climate and anthropogenic controls on blue carbon sequestration in Hudson River tidal marsh, Piermont, New York
 D Peteet, J Nichols, D Pederson et al.

ENVIRONMENTAL RESEARCH

LETTERS



OPEN ACCESS

RECEIVED

11 June 2021

REVISED

13 October 2021

ACCEPTED FOR PUBLICATION 20 October 2021

PUBLISHED

8 November 2021

Original Content from this work may be used under the terms of the Creative Commons Attribution 4.0 licence.

Any further distribution of this work must maintain attribution to the author(s) and the title of the work, journal citation and DOI.



LETTER

Expanding infrastructure and growing anthropogenic impacts along Arctic coasts

Annett Bartsch^{1,2,*}, Georg Pointner¹, Ingmar Nitze³, Aleksandra Efimova¹, Dan Jakober¹, Sarah Ley¹, Elin Högström¹, Guido Grosse^{3,4} and Peter Schweitzer^{2,5}

- b.geos, Industriestrasse 1, Korneuburg, 2100, Austria
- ² Austrian Polar Research Institute, Vienna, Austria
- Alfred Wegener Institute for Polar and Marine Research, Permafrost Research Section, Telegrafenberg A45, 14473 Potsdam, Germany
- University of Potsdam, Institute of Geosciences, Karl-Liebknecht-Str. 24-25, 14476 Potsdam, Germany
- University of Vienna, Department of Social and Cultural Anthropology, Universitätsstraße 7, 1010 Vienna, Austria
- * Author to whom any correspondence should be addressed.

E-mail: annett.bartsch@bgeos.com

Keywords: Arctic, permafrost, settlements, infrastructure, remote sensing, machine learning, Sentinel

Abstract

The accelerating climatic changes and new infrastructure development across the Arctic require more robust risk and environmental assessment, but thus far there is no consistent record of human impact. We provide a first panarctic satellite-based record of expanding infrastructure and anthropogenic impacts along all permafrost affected coasts (100 km buffer, ≈6.2 Mio km²), named the Sentinel-1/2 derived Arctic Coastal Human Impact (SACHI) dataset. The completeness and thematic content goes beyond traditional satellite based approaches as well as other publicly accessible data sources. Three classes are considered: linear transport infrastructure (roads and railways), buildings, and other impacted area. C-band synthetic aperture radar and multi-spectral information (2016–2020) is exploited within a machine learning framework (gradient boosting machines and deep learning) and combined for retrieval with 10 m nominal resolution. In total, an area of 1243 km² constitutes human-built infrastructure as of 2016–2020. Depending on region, SACHI contains 8%–48% more information (human presence) than in OpenStreetMap. 221 (78%) more settlements are identified than in a recently published dataset for this region. 47% is not covered in a global night-time light dataset from 2016. At least 15% (180 km²) correspond to new or increased detectable human impact since 2000 according to a Landsat-based normalized difference vegetation index trend comparison within the analysis extent. Most of the expanded presence occurred in Russia, but also some in Canada and US. 31% and 5% of impacted area associated predominantly with oil/gas and mining industry respectively has appeared after 2000. 55% of the identified human impacted area will be shifting to above 0 °C ground temperature at two meter depth by 2050 if current permafrost warming trends continue at the pace of the last two decades, highlighting the critical importance to better understand how much and where Arctic infrastructure may become threatened by permafrost thaw.

1. Introduction

Global warming is driving wide spread degradation of the Earth's cryosphere and warming in the Arctic is more pronounced than the global average (IPCC 2021). About 3.3 Million people are living in permafrost regions in the Arctic according to Ramage *et al* (2021). Warming of the Arctic results in widespread increase of ground temperatures

(Biskaborn *et al* 2019) and permafrost degradation is occurring in many regions (e.g. Hjort *et al* 2018, IPCC 2019). Expansion of thermokarst features has been also documented related to expanding infrastructure (Raynolds *et al* 2014). The length of the open water season has been increasing over the Arctic leading to increased capacity for coastal erosion (Barnhart *et al* 2014). Arctic coastal communities are seen as specifically vulnerable to climate change due to the combined

effects of sea ice loss and permafrost thaw (Irrgang et al 2019) which add to the non-climatic factors that require communities to adapt (Ford et al 2015). The latter affects the vulnerability of local and indigenous populations, increasing sensitivity to climate change impacts and constraining adaptive capacity (Ford et al 2015). The impact with respect to the economic value of ecosystem services, minerals and oil needs to be considered (O'Garra 2017). A wide range of geospatial data can be used to support vulnerability mapping including information on infrastructure such as roads (Preston et al 2011). Risk assessment frameworks which have been recently in focus for the Arctic (Larsen et al 2021) include physical exposure as one crucial element. The operability of such frameworks presuppose that, for example, the location and extent of infrastructure objects (settlements as well as transport infrastructure) under risk is known.

Ramage et al (2021) considered the locations of settlements for which population data have been available. Other risk assessment frameworks consider a much broader definition of the human footprint. Also, roads, railways, buildings, and airport strips are included (Suter et al 2019). Hjort et al (2018) for example utilize OpenStreetMap (OSM) data to represent built infrastructure on permafrost within a risk assessment framework. This allows for the consideration of infrastructure such as roads. However, the nature of this type of database results in inconsistencies. To account for such inconsistencies, specifically regarding minor roads, Hjort et al (2018) included only roads of a certain importance. In addition, as in similar studies, only roads and buildings excluding the surrounding grounds were considered part of the infrastructure. The infrastructure footprint in Arctic regions includes, however, also gravel pads and mines (excavation sites) as surface types (Raynolds et al 2014). In addition, large parts of the Arctic and specifically recent industrial development is not reflected in OSM (Bartsch et al 2020a). A consistent record which considers all relevant features is still lacking across the Arctic. The increasing human impact due to industrial development (e.g. Kumpula et al 2012) and military activities also remains to be quantified.

Satellite data can potentially be used to improve detection of infrastructure indicating human activities and also to categorize affected areas in Arctic environments. This includes high resolution optical satellite data (Kumpula *et al* 2012), the combination with synthetic aperture radar observations (Bartsch *et al* 2020a) as well as night-time light radiance records (Bennett and Smith 2017). There are, however, clear limitations. Impacts to natural assets that provide ecosystem services that are critical for survival and well-being of Arctic residents cannot be addressed and are beyond the scope of this paper.

Here, it deserves to be mentioned that infrastructures and other human impacts on the environment are not inventions of settler colonists. Limiting ourselves to transport infrastructure, indigenous networks of trails (Aporta 2009), the seasonal use of rivers, etc needs to be mentioned. The specific consideration of settler infrastructures in this paper is prompted by their size and quantity, which makes them detectable through remote sensing.

The aims of this study are (1) to quantify change of recent human impact in the panarctic coastal zone, specifically new infrastructure since 2000, (2) identify built infrastructure potentially impacted by recent climate change through combination with permafrost time series (Obu *et al* 2021a, 2021b, 2021c), and (3) to document the added value of satellite-derived built infrastructure maps along the Arctic coasts compared to datasets by OSM (Ramm 2020), night-time lights information (Elvidge *et al* 2021), and a recently published settlement dataset for the Arctic (Ramage *et al* 2021, Wang *et al* 2021). As a basis (aim #1), the algorithms of Bartsch *et al* (2020a) and Nitze *et al* (2018) are applied across the entire Arctic and a fusion and post-processing scheme is developed.

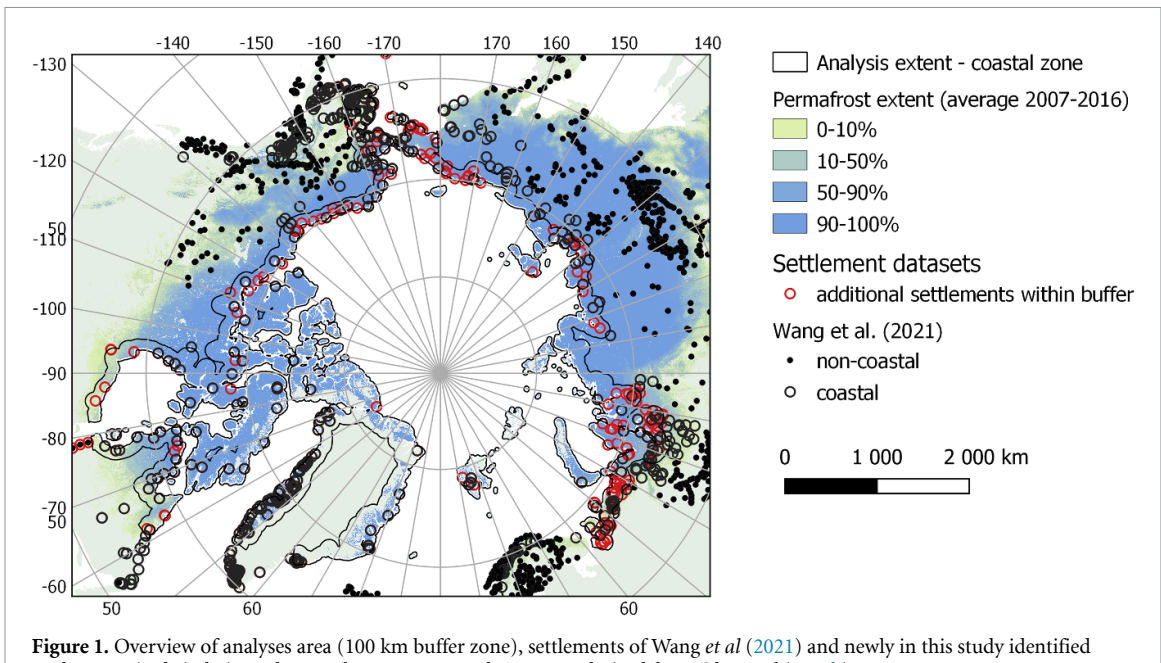
2. Study area and data

2.1. Arctic coasts

The extent of our analysis domain is defined by the spatial distance from the Arctic coast and by the presence of at least partially discontinuous permafrost (based on Obu et al 2021b). We chose a 100 km buffer from the coast to also include communities upstream from estuaries across the Arctic, which to some extent depend on sea access downstream (e.g. Cherskii in northern Yakutia). Compared to the socio-ecological system definition approach by Ramage et al (2021) and Wang et al (2021) (consideration of coastal dependence of settlements as defined by expert assessment), our approach excludes settlements located along the southern Alaskan coast, most of Scandinavia, the southern Newfoundland coast at the Atlantic Ocean, and several Russian settlements south of the treeline. The analyses extent covers approximately 6.2 Mio km². Figure 1 shows the extent and boundaries for our study area and location of settlements.

2.2. Data

A combination of Sentinel-1 (Synthetic Aperture Radar—SAR) and Sentinel-2 (multispectral-optical) was recommended by Bartsch *et al* (2020a) for human footprint identification in Arctic environments using the gradient boosting machines method, a machine learning approach applicable in data sparse regions (Chen and Guestrin 2016, Georganos *et al* 2018). An approach using Sentinel-2 only was suggested by the



settlements (red circles). Background: average permafrost extent derived from Obu et al (2021b).

same authors for the use of the Keras deep learning framework. For our study of panarctic coastal infrastructure mapping we therefore used both Sentinel sensor types (for details see appendix A).

Sentinel-1 data for winter time (exclusion of moisture impact on backscatter; December and early January) were assembled for winters 2017/2018 in 90% of all processed scenes, but also for 2018/2019 and 2019/2020 in some cases.

Sentinel-2 is provided in granules of a size of 100 km. More than 1200 granules overlaped with our 100 km buffer area along the coast, but less than 300 did overlap with inhabited areas. In total 2424 granules from years 2016 to 2020 were used in our study.

We used Landsat data for the quantification of normalized difference vegetation index (NDVI) trends in association with infrastructure change since 2000. The combined archive of Landsat-7 and -8 datasets formed the basis for trend analyses using multispectral indices as described in Nitze and Grosse (2016).

Auxiliary datasets included OSM (Ramm 2020), ground temperature data from the European Space Agency's (ESA) climate change initiative (CCI) permafrost project (Obu et al 2021a, 2021b, 2021c), a global night-time lights dataset (Elvidge et al 2021) and an Arctic settlements dataset (Wang et al 2021) (for details see appendix A).

To validate the Sentinel-1 and Sentinel-2 infrastructure classifications, Bartsch et al (2020a) used vectorized data on infrastructure based on high resolution observations of Prudhoe Bay and for several settlements with built infrastructure on Greenland and Longyearbyen. The Prudhoe Bay and Longyearbyen datasets (for sources see table A1) are used in this study to assess the quality of the post-processing scheme, specifically the impact of different editors.

3. Methods

3.1. Pre-processing and classification

An existing processing chain (Bartsch et al 2020a) was used as a first step to obtain results from two different classification approaches. It includes a pixel-based classification using a Gradient Boosting Machine (Chen and Guestrin 2016) and a windowed semantic segmentation approach (U-Net convolutional neural network architecture) using the deep learning framework Keras (Chollet 2017) with the Tensorflow backend. The approaches will be referred to as GBM and DL, respectively, in the following. The GBM is pixel based and the selected scheme provided three classes for human-affected areas and two classes for other features (vegetated tundra and open water). In contrast, the Keras DL framework allows for a more contextual approach and three classes only covering the target object types (human-affected area) were produced.

3.2. Post-processing and fusion of infrastructure

As demonstrated by Bartsch et al (2020a), misclassifications frequently occur for bare areas in case of the GBM approach. This includes lake and sea shores, river banks and exposed bedrock. Using, for example, Google hybrid maps such obvious misclassifications can be manually removed. The raster information was therefore converted to vector to allow object-specific editing. GBM results also included the classes 'other/tundra' and 'water bodies'. Both were

excluded from further analyses. All single pixel objects were removed automatically before manual removal involving several editors. The latter was carried out by four editors independently for selected sites to test the impact of possible performance differences. The same validation data as considered in Bartsch *et al* (2020a) was then used to assess the quality of the manual post-processing for Prudhoe Bay and Longyearbyen (Walker *et al* 2014, Lu *et al* 2018).

After clean-up, the outputs from DL and the GMB were fused. DL was given priority in the fusion process due to its better performance. In case of presence of an object identified with DL, the objects from GBM are dropped. Automatic fusion was carried out using the Python package 'geopandas' (Jordahl *et al* 2021). In the following step, polygons were dissolved by human impact class. Since there are overlaps between adjacent Sentinel-2 granules, polygons of different classes could still overlap after the dissolve step. Where there was still overlap, differences were calculated using polygon sets for each class to allow only one polygon of a certain class at a single location. During this step, highest priority was given to the building class, followed by the road class.

3.3. Preparation of auxiliary datasets and combination

A Theil-Sen regression (Sen 1968, Theil 1992) was used for trend retrievals from 2 m ground temperature, active layer thickness (ALT), and permafrost fraction. In case of Landsat derived NDVI, the trends have been obtained with Ordinary Least Square regression. For NDVI, changes per decade, and for all other parameters, changes per year were extracted. For each object the average change was derived. This was carried out for all classes together as well as separately. The analyses were made on different levels: the entire Arctic and by country/region (in both cases subset with the 100 km buffer).

NDVI change occurs due to climate change (greening, rapid permafrost thaw) and hydrologic processes as well as human impacts. A certain magnitude of abrupt negative change can be expected in the latter case. A value of 0.6 is a common NDVI for Tundra in case of high shrub cover, but it can also be lower; less than 0.3 is typical for bare ground (Bartsch *et al* 2020b). An NDVI trend of smaller than -0.1 per decade was therefore chosen as threshold for identification of impacted areas.

All objects were assigned settlement names and further attributes where available. In a first step the settlement database of Wang et al (2021) was used. A 40 km search radius was applied. Clusters of objects which remained unassigned were manually reviewed in a second step. Missing settlements were identified and added, guided by information from the Google Hybrid data layer. The updated settlement database was then extended for name and economic use/function based on information accessible on the

internet. The following general categories were considered: fishing, agriculture (mostly reindeer herding), gas/oil industry, mining, other use (e.g. transport hub), abandoned, and unknown (sub-categories are provided in table B1). It should be noted that this approach does not allow for distinction between, for example, subsistence-harvest and commercial fisheries or extractive industries overlapping with subsistence land use.

Eventually a 40 km maximum search radius (benchmark Bovanenkovo, Yamal) was applied to all objects again in order to attribute the mapped features to a certain settlement and to assign the economic use/function to them. This is of relevance for the comparison to the NDVI trends in order to analyze differences across different settlement and use types.

3.4. Comparison with OSM

OSM data contain a wide range of features. But specifically the road class comprises a diversity of transport routes. This includes also winter routes which do not rely on permanent constructions and therefore are mostly not visible in summer acquisitions of multispectral images. This needs to be considered for the comparison. Therefore, based on the mapped features, all relevant OSM objects (buildings, traffic, transport, railways, roads) were extracted to identify how much of our dataset is represented in OSM, but only buildings were analyzed for the extraction of satellite derived features based on the OSM. In order to account for positional inaccuracies in both datasets, buffers of 30, 50 and 100 m were used for the overlay analyses.

4. Results

4.1. Post-processing of infrastructure classifications

Three-hundred and sixty-six granules contained identifiable infrastructure. 99.5% of GBM results and 35.0% of DL results were manually removed. Deviations between different editors were less than $\pm 2.5\%$ (differences largest for roads, tables 1 and 2). The merged dataset provides a better producers accuracy for roads (60%) while keeping the values for natural areas high (95%; see table 3). The results from Prudhoe Bay (producers accuracy) for 'impacted' areas demonstrated the added value of merging DL and GBM. While DL provided very good results for roads it had low performance for other 'impacted' areas. The producers accuracy for Longyearbyen suggests better performance of DL alone, but the users accuracy could not be derived in this case (table 4). The manual editing specifically improved the GBM results (both sites) and allowed for an enhancement through the merging.

Table 1. Users and producers accuracy of post-processed results (by four different editors A–D) of DL (deep learning) and GBM (gradient boosting machines) for Prudhoe Bay. Reference dataset: Walker *et al* (2014) with separation of non-impacted (56.41 km²), impacted (4.16 km²), roads (1.44 km²).

		Producer accuracy				User accuracy				
Method	Editor	Road	Building as 'impacted'	Other as 'impacted'	Natural	Road	'Impacted' as building	'Impacted' as other	Natural	
DL	A	54%	95%	77%	93%	35%	5%	11%	99%	
	В	54%	95%	77%	93%	35%	5%	11%	99%	
	C	54%	95%	77%	93%	35%	5%	11%	99%	
	D	54%	95%	77%	93%	35%	5%	11%	99%	
GBM	A	28%	80%	56%	98%	44%	33%	30%	97%	
	В	28%	80%	57%	98%	45%	33%	30%	97%	
	С	28%	80%	58%	98%	44%	33%	30%	97%	
	D	28%	80%	57%	98%	45%	33%	30%	97%	

Table 2. Producers (per reference class) accuracy of post-processed results (by four different editors A–D) of DL (deep learning) and GBM (gradient boosting machines) for Longyearbyen. Reference dataset: Lu et~al~(2018) with 0.13 km 2 for roads and buildings and 0.42 km 2 for natural areas.

Method	Editor	Road	Building	Natural
DL	A	98.10%	96.51%	100.00%
	В	98.10%	96.51%	100.00%
	С	98.10%	96.51%	100.00%
	D	98.10%	96.51%	100.00%
GBM	A	46.65%	85.27%	100.00%
	В	48.52%	85.27%	99.98%
	С	44.96%	85.40%	100.00%
	D	49.71%	85.27%	100.00%

Table 3. Users and producers accuracy of the merged product, original and post-processed results (average of four different editors, see table 1) of DL (deep learning) and GBM (gradient boosting machines) for Prudhoe Bay. DL-original refers to results of Bartsch *et al* (2020a). Reference dataset: Walker *et al* (2014) with separation of non-impacted (56.41 km²), impacted (4.16 km²), roads (1.44 km²).

	Producers accuracy				Users accuracy			
Product	Road	Building as 'impacted'	Other as 'impacted'	Natural	Road	'Impacted' as building	'Impacted' as other	Natural
DL-original	54.00%	95.00%	77.00%	93.00%	35.46%	5.09%	11.10%	97.85%
DL postprocessed (average)	53.87%	94.81%	76.88%	92.96%	35.36%	5.01%	10.96%	99.28%
GBM-original	24.00%	78.00%	38.00%	99.00%	46.46%	33.87%	31.52%	76.77%
GBM postprocessed (average)	28.20%	80.07%	57.03%	97.95%	44.75%	33.15%	30.37%	96.89%
Final product	26.04%	79.50%	64.68%	98.46%	69.37%	28.29%	31.21%	95.46%

Table 4. Producers accuracy of the merged product, original and post-processed results (average of four different editors, see table 1) of DL (deep learning) and GBM (gradient boosting machines) for Longyearbyen, Svalbard. DL-original refers to results of Bartsch *et al* (2020a). Reference dataset: Lu *et al* (2018).

Product	Road	Building	Other
DL-original	65%	75%	100%
DL-postprocessed (averaged)	98%	97%	100%
GBM-original	55%	36%	61%
GBM-postprocessed (averaged)	47%	85%	100%
Final product	57%	95%	100%

4.2. Post-processed settlements data base

The settlement dataset of Wang *et al* (2021) contained 285 settlements within our analyses extent. 47% of all objects could be directly assigned to them. After the semi-automatic extension (addition of 221 settlements based on identified clusters within our results, figure 1), 87% could be attributed. Remaining objects

correspond mostly to roads and railways connecting the remote locations.

4.3. Human-impacted area across the Arctic

In total, 0.02% of the land area within the 100 km buffer was identified as human-impacted (sum of all target classes). The overall sum is 1243 km².

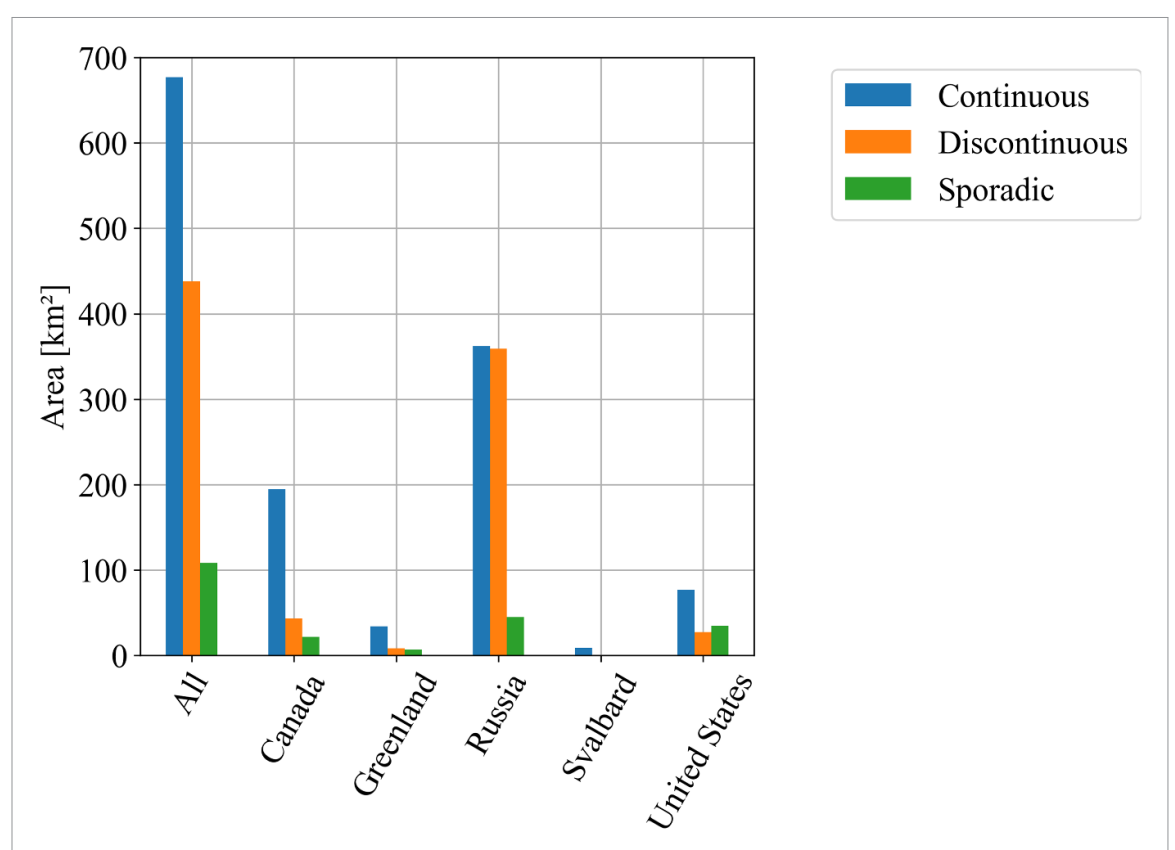


Figure 2. Distribution of human-impacted area as mapped with Sentinel-1 and -2 within the analysis extent across different permafrost zones by country/region (year 2019, permafrost zone source: Obu *et al* (2021b)). For analyses extent see figure 1.

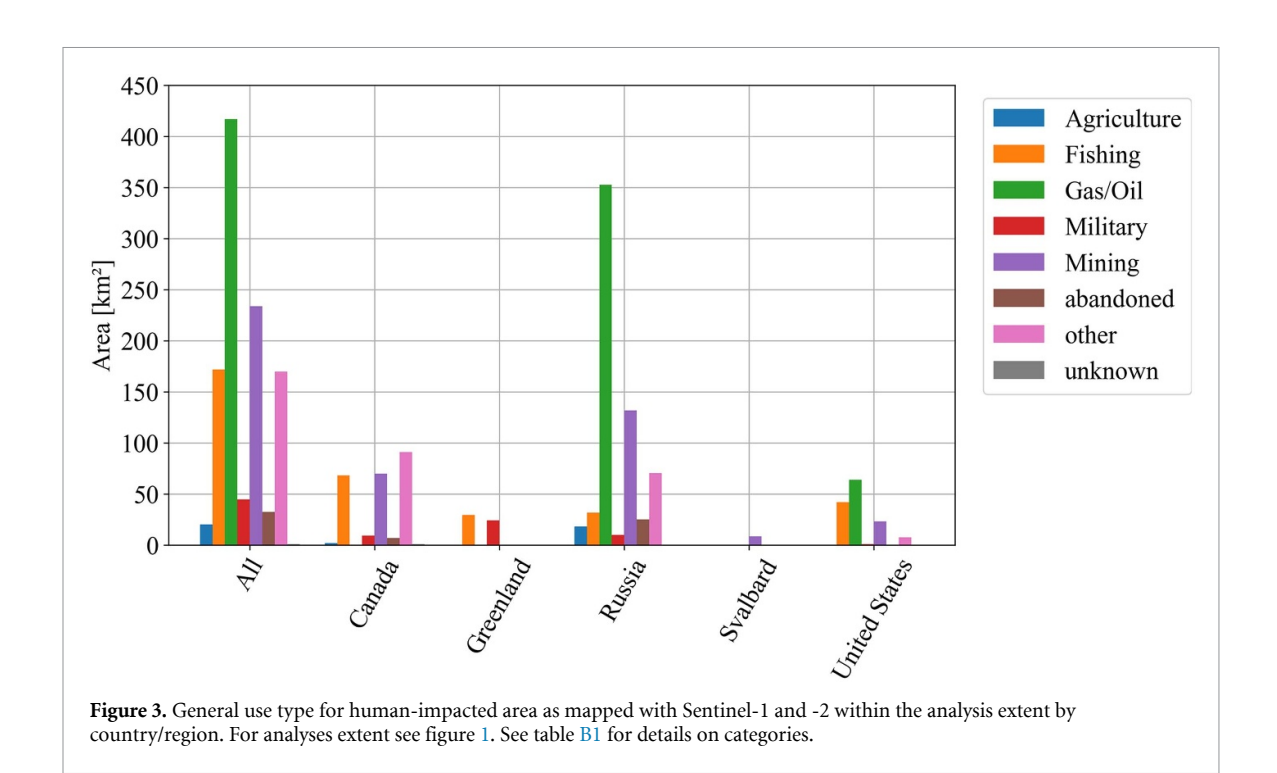
Table 5. Distribution of human-impacted areas in absolute and relative values (with respect to sum of identified areas within the 100 km Arctic coastal zone) and proportion of NDVI reduction of more than 0.1 per decade by country/region for 2000–2018.

Туре	Roads	Buildings	Other impacted areas
Area in km ²	661	204	378
Proportion in %	54	16	30
NDVI decline in %			
Canada	5.7	8.7	8.7
Greenland	0.9	1.9	1.0
Russia	15.4	14.4	28.8
Svalbard	18.2	7.6	26.1
United States	3.4	6.1	11.7

More than 50% occurs over continuous permafrost and more than 30% over discontinuous permafrost (figure 2). Most identified areas in Canada and US are located on continuous permafrost. For Russia this applies to less than half of them. The majority of the human-impacted area was assigned to the 'Road' class and least to 'Buildings' (table 5). Most of the human impacted areas that we identified relate to oil/gas industry and mining activities (figure 3). It needs to be noted that there might also be subsistence land use in the surroundings. On average, 31% of area associated with oil/gas (overall occurrence 38%) is new since 2000 and 5% in case of mining (overall occurrence 21%) (figure 5).

The NDVI trend with the maximum frequency is positive (figure 4(a)) and the total area with a positive trend is also larger than with a negative trend (789 km² versus 454 km², respectively). The average is, however, close to zero (-0.006 per decade). Larger changes (greater than 0.1) are less common and differ between regions (figures 5 and C1, table 5). As an example, greening seems to occur for Svalbard settlements with at the same time a decline at the same magnitude due to extension of infrastructure. Greening dominates around Longyearbyen, Ny Alesund and Pyramiden and a decline around the mining towns of Svea and Barentsburg (figure 6). A notable partial NDVI decline can be observed for all regions except Greenland (figures 5 and C1). The affected area and proportion is largest for Russia. Most relates to infrastructure expansion in Western Siberia (figure 7) and in general to gas and oil industry (figure 8). In total, 159 km² are affected in Russia, compared to 19 km² for Canada and 9 km² for US. Most falls into the categories 'roads' and 'other' (figure C1).

Almost 97% of all mapped areas showed a positive trend in ground temperature and 93% for ALT (figures 4(b) and (c)). Temperatures were increasing by 0.8 °C per decade on average over the humanimpacted area identified within the analysis extent. The ALT increase was 11 cm per decade (average ALT in 2019 was 84 cm). About 8% changed from a permafrost fraction of 100% to a lower value between 1997 and 2019.



The changes in ground temperature during the last two decades tend to be larger in colder permafrost than for ground with temperatures near zero degree C (as determined for the year 2019, figure 9), which agrees with prior findings (Romanovsky *et al* 2017, Biskaborn *et al* 2019, Box *et al* 2019). As the magnitude for the latter is still on the order of one degree C for this time period, the expected impact during the upcoming decades is large if the trend continues. 55% and 67% of human-impacted areas will be located on ground with larger than zero degree C mean annual ground temperature down to 2 m depth in 2050 and 2060 respectively. Most affected is Russia and some areas in the US (Alaska) (figures 11 and C2).

4.4. Night-time lights comparison

Approximately 53% of the overall identified humanimpacted area was represented in the night-time light dataset (3% had no data, 44% had a radiance value of 0 nW cm⁻² sr⁻¹). This overlap was similar across all considered classes, with only a slightly lower fraction for buildings. The uncovered areas included 48% of the roads or rail tracks, 47% of the other human impacted areas, and 42% of the buildings class. The latter were often constructions in association with pipelines and railroads. It also included misclassifications of road segments.

The most frequent night-time light radiance was around $10 \,\mathrm{nW}\,\mathrm{cm}^{-2}\,\mathrm{sr}^{-1}$ (figure 4). It was derived from all regions where data is available (figure 10; Svalbard is not included in Elvidge *et al* 2021). It was higher for Greenland (about $20 \,\mathrm{nW}\,\mathrm{cm}^{-2}\,\mathrm{sr}^{-1}$) and lower for Russia and US (around $6-7 \,\mathrm{nW}\,\mathrm{cm}^{-2}\,\mathrm{sr}^{-1}$).

The maximum for Greenland was 40, for Canada 90, and for the US about $700 \,\mathrm{nW}\,\mathrm{cm}^{-2}\,\mathrm{sr}^{-1}$. A value of $1000 \,\mathrm{nW}\,\mathrm{cm}^{-2}\,\mathrm{sr}^{-1}$ per object was only exceeded for Russia. Such a high radiance occurred over 0.7 km². The overall average radiance for objects with data was $26 \,\mathrm{nW}\,\mathrm{cm}^{-2}\,\mathrm{sr}^{-1}$.

4.5. OSM comparison

In total, 40% of human-impacted area identified in SACHI was not yet included in OSM. This value is lowest for Svalbard (8%) and highest for Russia (48%) considering a 100 m buffer (table 6). About 18% of buildings contained in the OSM have not been identified as human-impacted considering a radius of 100 m.

5. Discussion

The combination of Sentinel-1 and Sentinel-2 as well as the GBM and DL approach provides a means for quantification of human-impacted areas in the permafrost affected Arctic coastal zone. But a range of limitations needs to be considered when using the resulting SACHI dataset for further analyses. Many smaller unpaved tracks which are very common in the Arctic (Kumpula *et al* 2012, Ehrich *et al* 2018) cannot be captured due to the spatial resolution limits. The same applies to winter roads (seasonal ice roads) which play an important role in the Arctic, but cannot be readily detected with summer season imagery. In general, the 'road' class which encompasses linear infrastructure also including rail tracks has a rather low accuracy based on the chosen validation datasets

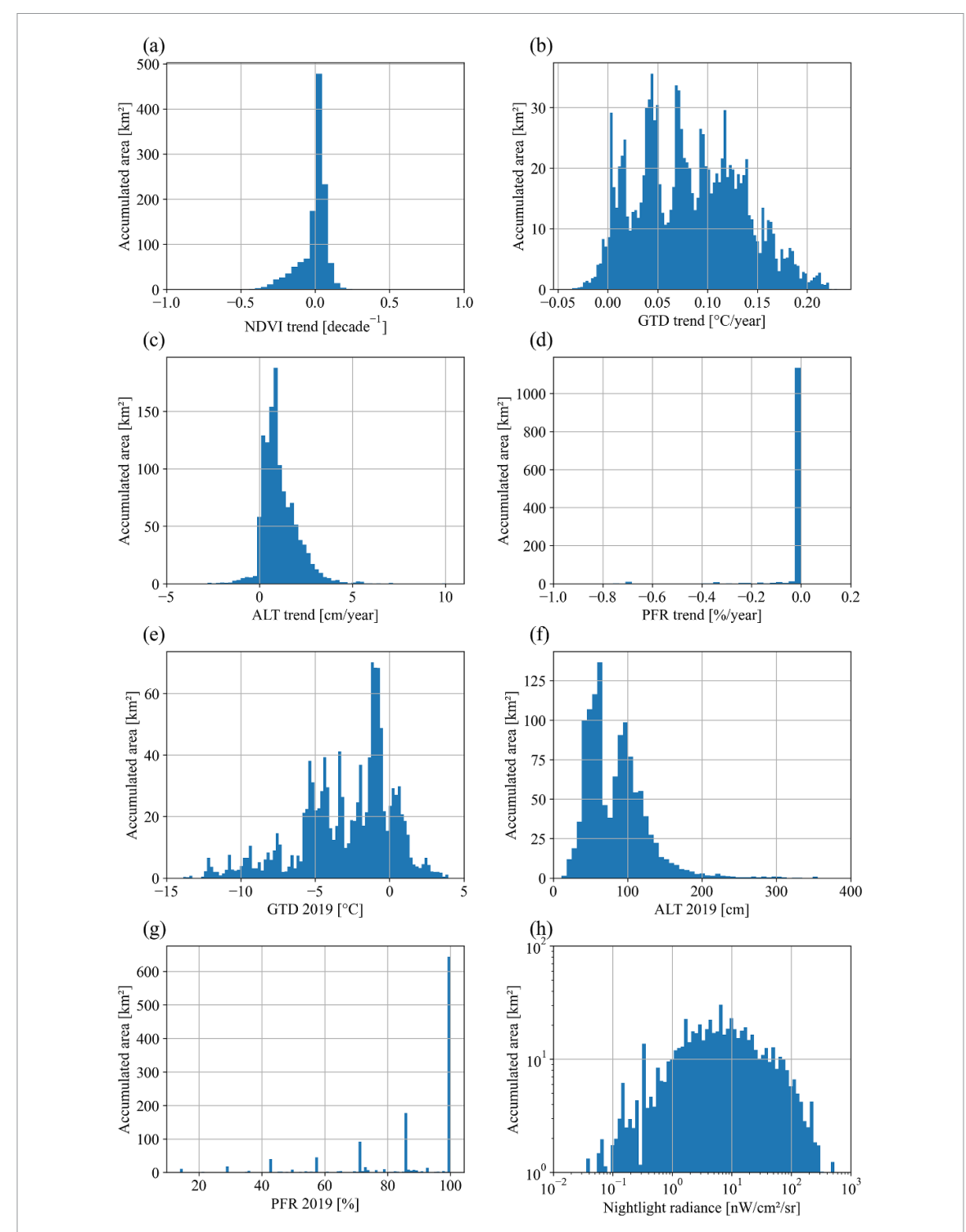


Figure 4. Histograms for selected trends and states within the human-impacted area as mapped with Sentinel-1 and -2: (a) normalized difference vegetation index (NDVI) trends 2000–2018 $\varnothing=-0.006$), (b) ground temperature (GTD) trend at 2 m depth 1997–2019 ($\varnothing=-0.08\,^{\circ}\mathrm{C}\,\mathrm{yr}^{-1}$), (c) active layer thickness (ALT) trend 1997–2019 ($\varnothing=-1.1\,\mathrm{cm}\,\mathrm{yr}^{-1}$), (d) permafrost fraction (PFR) trend 1997–2019 ($\varnothing=-0.23\%$), (e) Ground temperature at 2 m depth in 2019 ($\varnothing=-2.9\,^{\circ}\mathrm{C}$), (f) active layer thickness 2019 ($\varnothing=84cm$), (g) Permafrost fraction 2019 ($\varnothing=85.9\%$), (h) Night-time light radiance 2016 (Elvidge *et al* 2021) for the mapped areas ($\varnothing=26.3\,\mathrm{nW}\,\mathrm{cm}^{-2}\,\mathrm{sr}^{-1}$). Sources of permafrost values (b)–(g): Obu *et al* (2021a, 2021b, 2021c).

(tables 3 and 4). The 10 m resolution is very limiting but still provides a step forward for infrastructure mapping in Arctic environments. Further, Bartsch *et al* (2020a) noted that the performance of HH versus VV polarization for the Gradient Boosting Machines

approach differs. This may affect results from Greenland. However, our approach to fuse GBM with the Deep Learning results helps to limit the impact of some of the differences. If only linear infrastructure is of interest, then the application of Deep Learning

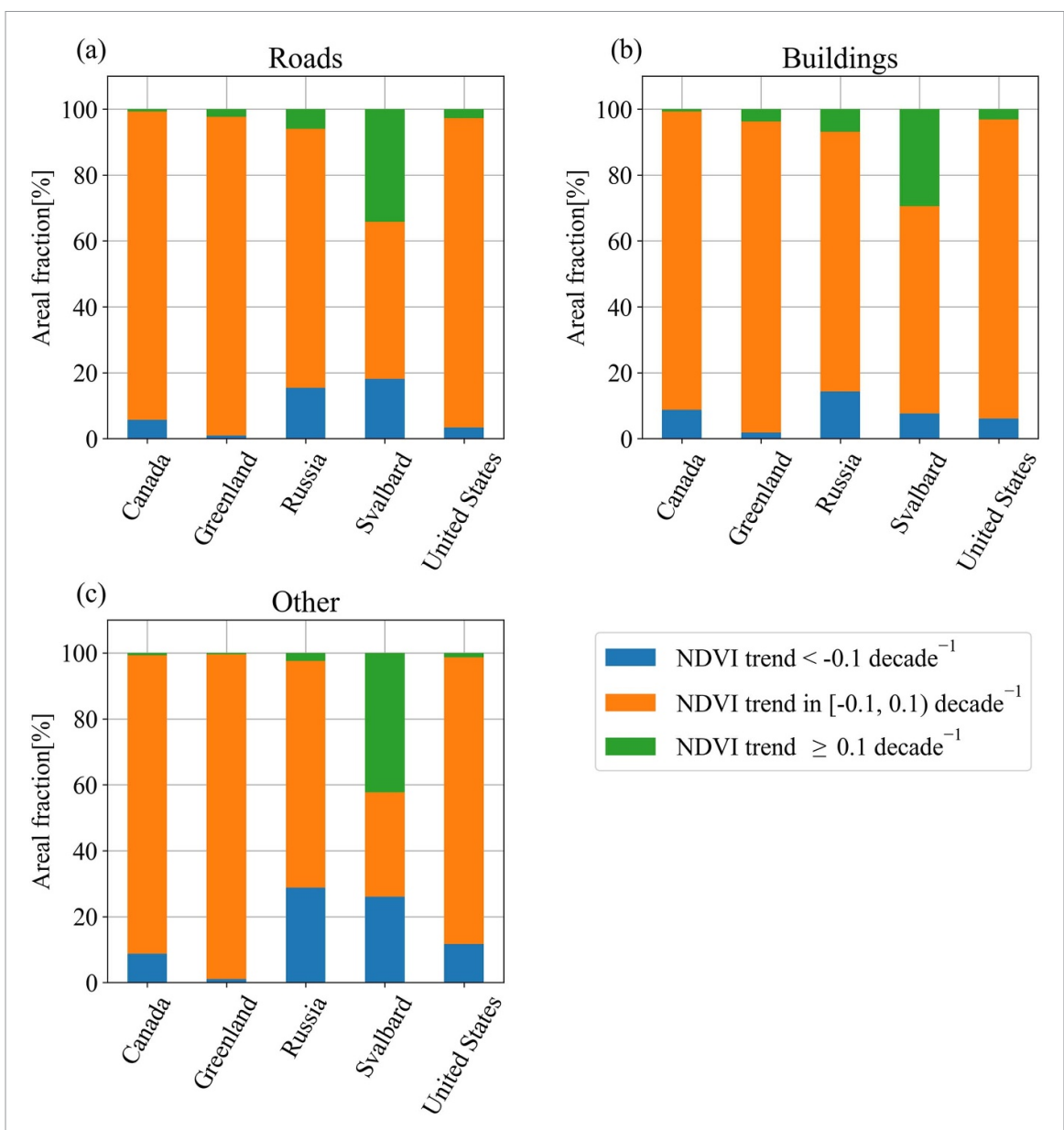


Figure 5. Fraction of Landsat-based normalized difference vegetation index (NDVI) change trends 2000–2018 for each class of human impacted area as mapped with Sentinel-1 and -2 by country/region.

might be sufficient (tables 3 and 4). Other impacted areas such as open pit mines are irregularly shaped and can not yet be well captured with DL (users accuracy table 3). A revision of the training of the algorithm and extension of target classes to reflect different possible 'other impacted' areas might allow for improvements.

Three issues need to be considered when interpreting the NDVI trends: (1) the retrieval of zonal statistics by object may cause object size-dependent effects, (2) the mismatch of spatial resolution between Sentinel-1/2 and Landsat, and (3) the range of NDVI levels across different Arctic landscapes. As NDVI is derived for specific objects, smaller features such as buildings have fewer pixels and thus are more likely to be assigned extreme changes while larger objects

may be less represented through extreme changes because a larger number of pixels averages out strong change. This is especially relevant for road networks (also connecting to runways, as e.g. in Longyearbyen, figure 6(b)). But due to the fact that NDVI change is derived from a coarser resolution dataset which does not resolve roads, also a pixel based retrieval is not expected to provide more locally representative values in most cases. The mixed pixel effect likely has a larger effect on roads than on square gravel pads. Hence, variations between objects may not in all cases reflect an actual degree of vegetation removal. It is therefore suggested to derive change/no change only from the SACHI dataset (as done in this study). The general background NDVI may also differ between regions and this should be considered. Extensions of built

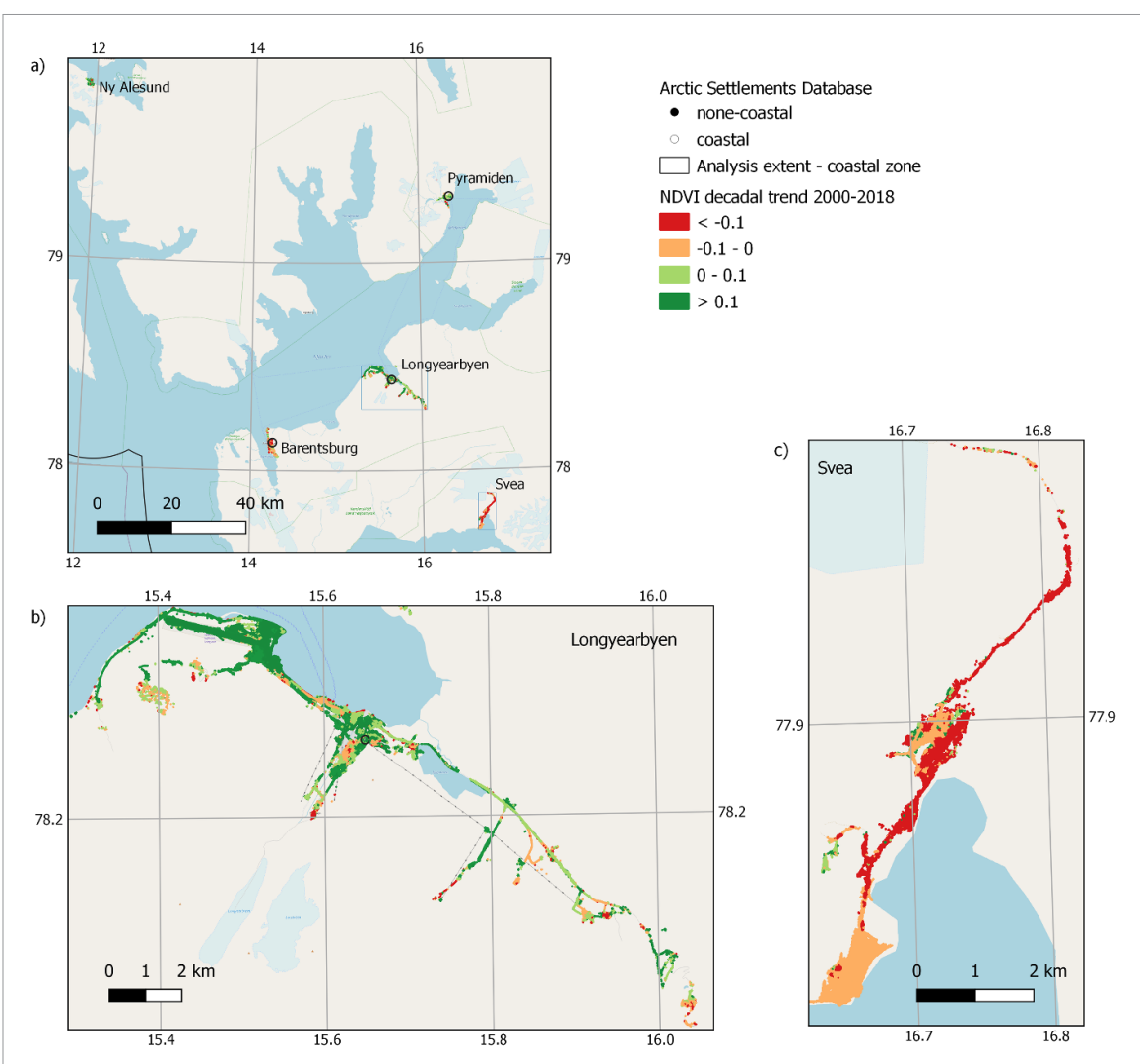


Figure 6. Landsat-based normalized difference vegetation index (NDVI) change 2000–2018 within human impacted areas as mapped with Sentinel-1 and -2 (averages for distinct objects) for (a) central Svalbard, (b) subset for Longyearbyen and (c) Svea (background: OpenStreetMap). Values less than -0.1 indicate new human impacts after 2000. Source of settlement locations: Wang *et al* (2021).

infrastructures on bedrock or other barren ground, for example in the High Arctic, might not reflect well in the NDVI trend values. Including other multispectral indices sensitive to soil moisture, such as the normalized different moisture index, may enhance such detection in future upgrades of the workflow. The focus for this study was on vegetation decline, but greening is also a common feature in Arctic settlements (see Svalbard example figure 6). Settlements with built infrastructure are in cases partially abandoned or vegetation recovers after disturbance due to construction works.

The magnitude of ground temperature change (figure 11) is similar to previous findings which focus on larger parts of the Arctic. Ramage *et al* (2021) estimate that about 42% of settlements currently on permafrost will experience widespread permafrost thaw by 2050. Hjort *et al* (2018) estimate based on statistical modelling of mean annual ground

temperature that 70% of all Arctic infrastructure will be affected by thaw by 2050 (RCP4.5 for 2041–2060). These estimates are, however, not directly comparable due to the different extent, less considered human-impacted areas, and differences in the retrieval for ground temperature projections for 2050 (2 m depth versus unspecified depth). The simple trend interpolation results specifically deviate in Western and Far Eastern Siberia (figure 11).

The permafrost temperature dataset used in this study is based on a modelling approach (Westermann *et al* 2015, Obu *et al* 2021c). Adequate soil parameterization is needed to represent heat transfer. Many artificial surfaces are currently not considered in such models. In case of larger areas with built infrastructure (with respect to the 1 km gridding of the permafrost data), temperatures and ALT might therefore deviate.

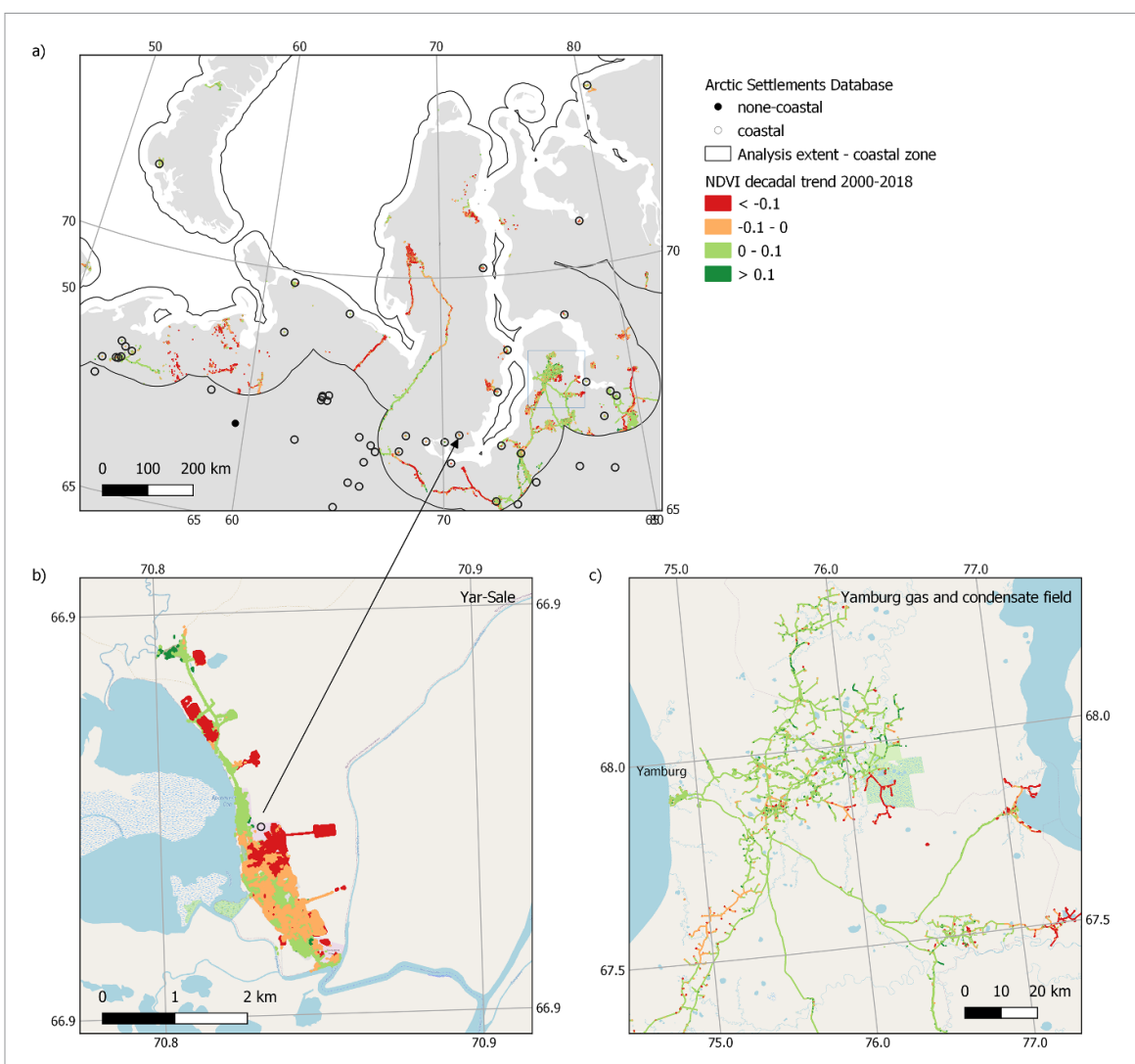


Figure 7. Landsat-based normalized difference vegetation index (NDVI) change 2000–2018 within human impacted areas as mapped with Sentinel-1 and -2 (averages for distinct objects) for (a) Western Siberia, (b) subset for Yar-Sale on the southern Yamal peninsula and (c) the Yamburg gas and condensate field (background of (b) and (c): OpenStreetMap). Values less than -0.1 indicate new human impacts after 2000. Source of settlement locations: Wang *et al* (2021).

15% of identified objects could not be assigned to a specific settlement. This, on the one hand reflects remoteness of some infrastructures for this region but might also be caused by the fact that a name could not be found for all object clusters, especially in Russia. Some of these settlements are not historically grown public places but they result from mining industry. Constructions related to mining, oil and gas industry typically extend over larger regions with a network of roads and pipelines which connect gravel pads or mines with industrial facilities (e.g. figure 7(c)). Use categories depend on availability of information. No category could be assigned in 47 cases. Those are most likely indigenous communities. It can also be assumed that not all landuse and economic activities are captured. Some settlements in Canada and Alaska have been assigned Tourism as the only category (figure B1) but subsistence land use such as hunting and fishing can be most likely

also expected. Mining and Gas/Oil industry use can be, however, clearly identified and thus features associated with indigenous communities outside these regions potentially separated. Such settlements are characterized by slightly increasing NDVI and low night-time light radiance values (table B1).

Owing to the OSM data model, there can theoretically be an infinite number of mappings from OSM data to discrete GIS layers. Here, we used the thematic layers extracted by Geofabrik. The mapping they used is described in detail by Ramm (2019). Certain layers, such as 'points of interest' or 'places' were available as point geometries, that could not be used in our analyses. Road data were available as linestring geometries only, which might potentially affect the comparisons to our results.

Elvidge *et al* (2017) note a background radiation of about $1 \,\mathrm{nW}\,\mathrm{cm}^{-2}\,\mathrm{sr}^{-1}$ in high latitudes. This reduces the features with night-time light

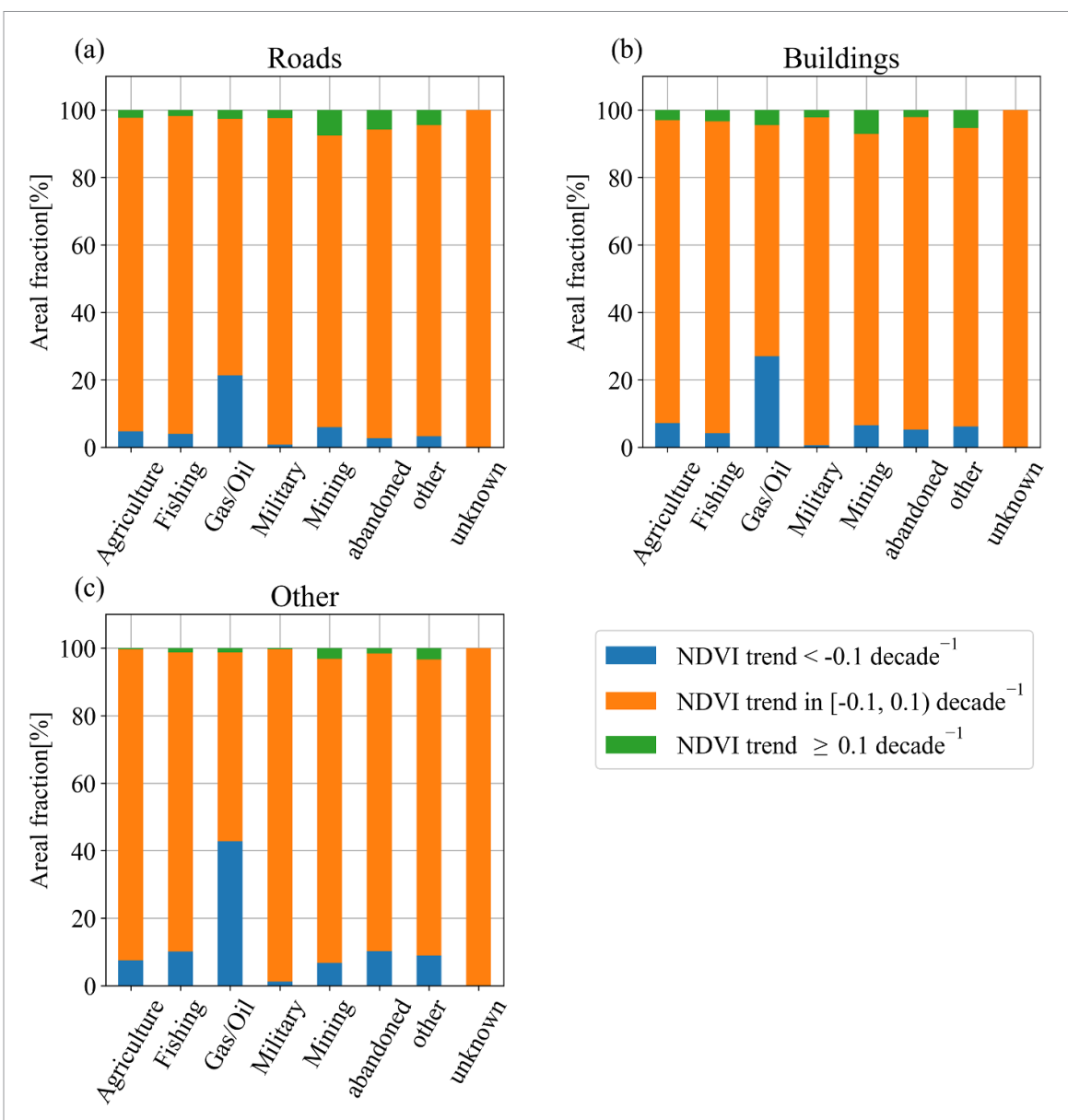


Figure 8. Landsat-based normalized difference vegetation index (NDVI) change 2000-2018 within human impacted areas as mapped with Sentinel-1 and -2 by general use type. Values less than -0.1 indicate new human impacts after 2000.

information further, to 44.9%. Large cities such as Seoul can have areas with radiance of larger than $100 \,\mathrm{nW}\,\mathrm{cm}^{-2}\,\mathrm{sr}^{-1}$ according to Elvidge et al (2021). About 3% of the human impacted area along the Arctic coasts has values higher than this. It occurs for example on the Prudhoe Bay Oil field in Alaska, Churchill in Canada and in many oil/gas industry settlements in Western Siberia. Bennett and Smith (2017) discuss the detection of gas flaring for Bovanenkovo (Yamal, Western Siberia). They exemplify the derivation of fixed capital investment (oil as well as non-oil producing) from night-time light properties for Russia. Future studies may therefore also consider the inclusion of night-time light trends for monitoring of industrial developments across the Arctic.

The identifiable features cover only a proportion of assets which are of relevance to local communities, providing limited insight for vulnerability studies (Fritz et al 2017, Brady and Leichenko 2020). The possibility to identify built infrastructure and population centers does nevertheless contribute to assessing Arctic exposures to global warming impacts. First, the pan-arctic scale allows comparisons between different regions and landuse types. Second, the extension of the features with resource use categories provides a first step for enhanced insight into regions with limited socio-economic diversity and proximity of indigenous communities to industrial developments. Natural assets (Brady and Leichenko 2020), symbolic values (Adger et al 2011) and societal limits to adaptation (Adger et al 2009, Ford et al 2015)

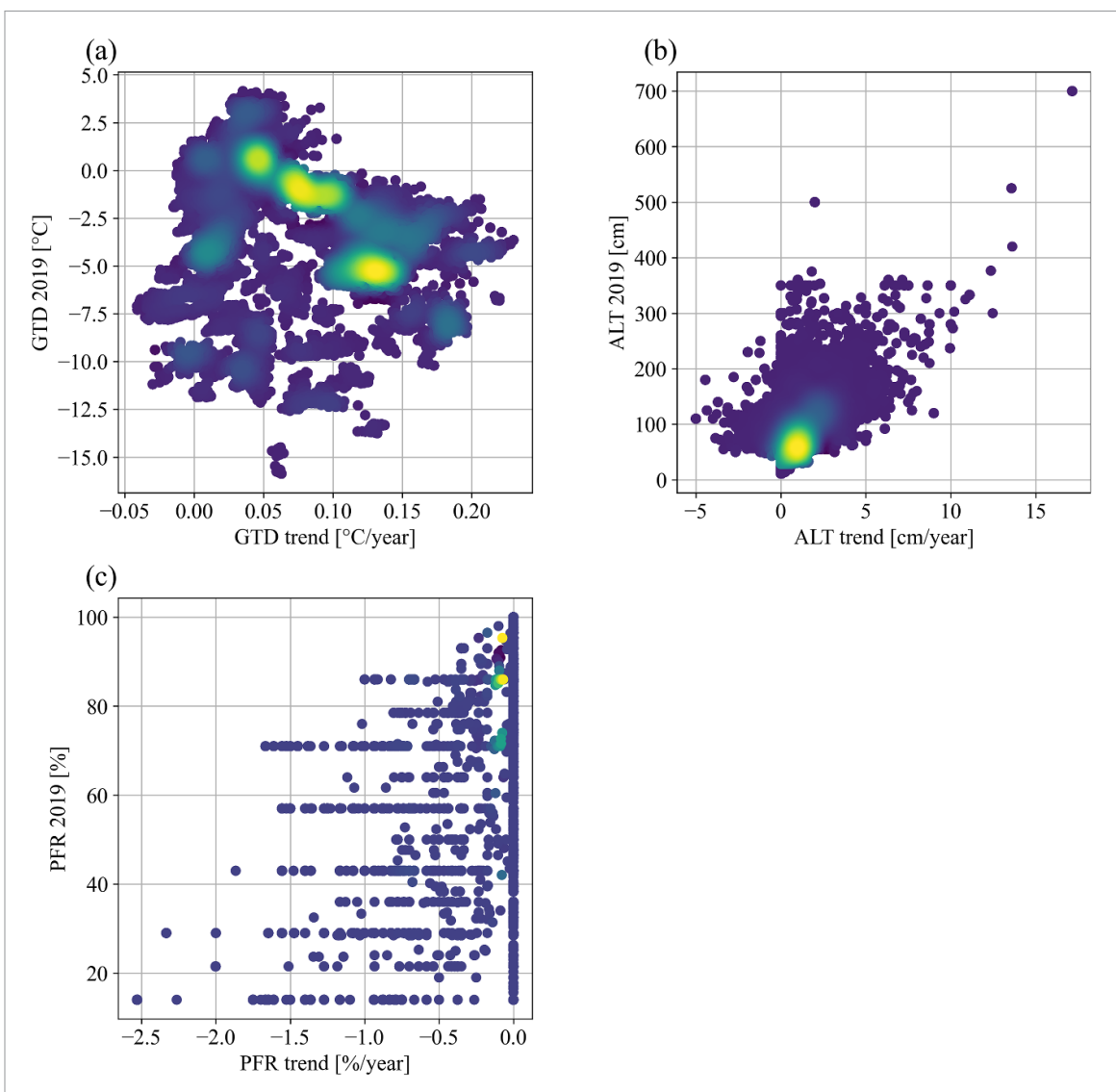


Figure 9. Scatterplots of trend versus 2019 status for (a) ground temperature at 2 m depth, (b) active layer thickness and (c) permafrost fraction. Each point represents the average for a distinct object (human impacted area) as mapped with Sentinel-1 and -2 (Bartsch *et al* 2021). Calculations are based on Obu *et al* (2021a, 2021b, 2021c) respectively.

are critical aspects of global warming impacts in the Arctic that are not captured in this study. It therefore provides only limited insight into what is at risk for local communities. Satellite derived information, however, may aid identification of natural assets but implementation at the Arctic scale (what would require a high degree of automatizing) is challenging. For example, while built infrastructure was the focus here, satellite information using other techniques can be used to detect coastal change, including barrier islands and other coastal features that are rich in wellmapped subsistence and related traditional land use in the Arctic.

The actual interpretation regarding the impacts on local communities cannot be uniformly handled for the Arctic. Country specific developments need to be considered. Some mining and hydrocarbon infrastructures are led by Native Corporations in Alaska

Table 6. Percentage of human impacted area not included in OpenStreetMap considering buffers of 30, 50 and 100 m.

Region	30 m	50 m	100 m
Canada	63 %	48 %	34 %
Greenland	53 %	38 %	26 %
Russia	68 %	58 %	48 %
Svalbard	43 %	22 %	8 %
Alaska	48 %	32 %	20 %

(Brady and Leichenko 2020) whereas such involvement is not documented for Russia. Overall, expanding infrastructure can be only observed for settlements with mining and gas/oil industry related use. While we can monitor the extent of impact, the quality of local impacts can only be assessed through *in-situ* fieldwork. It also needs to be considered that the development of the often externally controlled

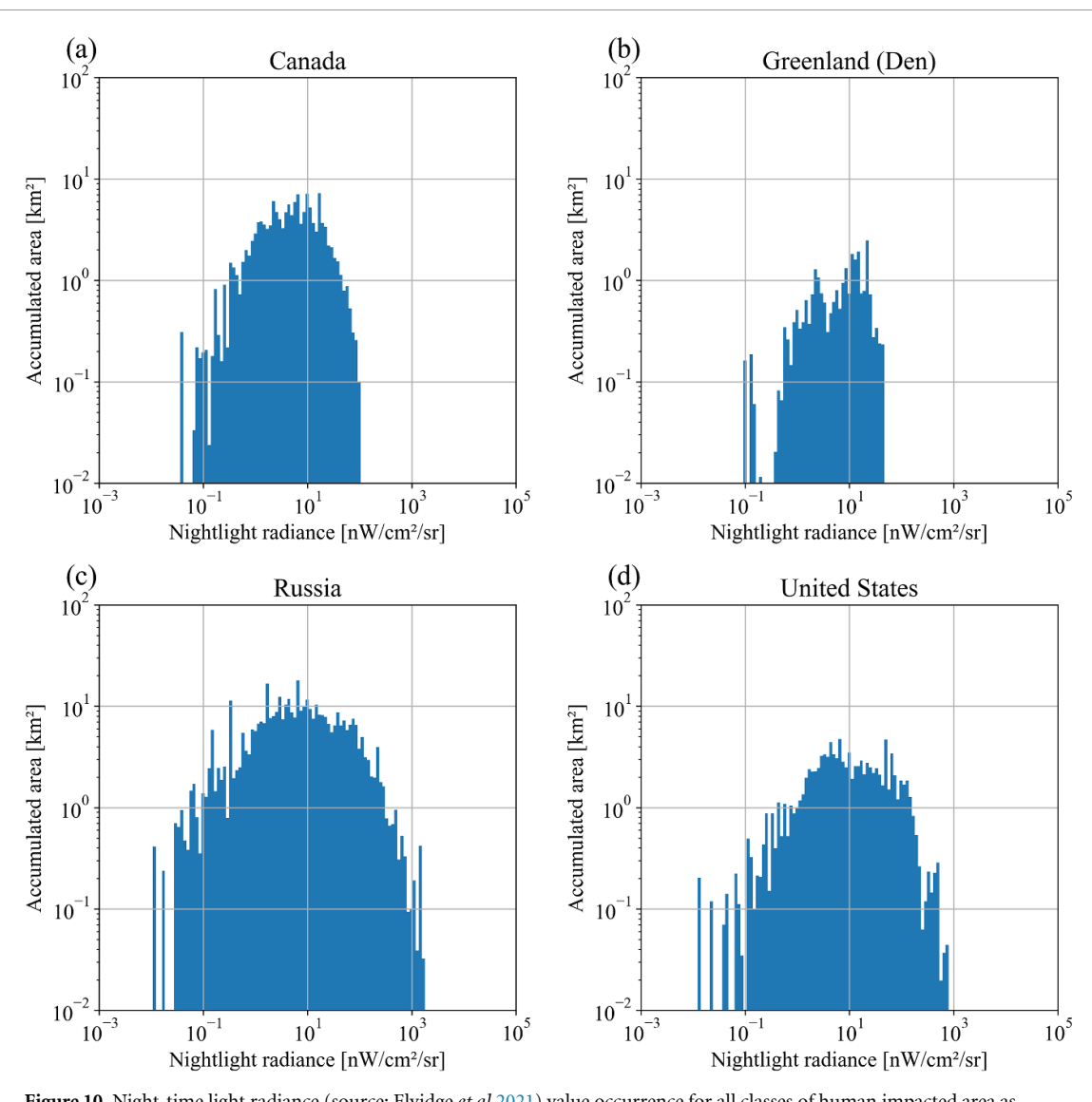


Figure 10. Night-time light radiance (source: Elvidge *et al* 2021) value occurrence for all classes of human impacted area as mapped with Sentinel-1 and -2 by country/region (analysis extent only).

extractive infrastructure adds to the vulnerability for local residents, in addition to climate change, leading to 'double exposure' (O'Brien and Leichenko 2000).

6. Conclusions

Positive ground temperature trends during the last two decades were observed for the vast majority of identified infrastructure objects. More than half of it will shift from permafrost to non-permafrost at 2 m depth by 2050 considering a simple ground temperature trend extrapolation.

The inclusion of natural assets which are of high relevance for local communities remains open and requires future research with respect to the utility of satellite data analyses. Nevertheless, the identification of infrastructure and population centers across the Arctic provides a step forward for human impact monitoring in Arctic environments. Sentinel-1/2

derived impacts on natural assets provide more detail than any other currently available records for this region. Conventional satellite derived information is confined to densely populated regions with built-up areas and therefore the Far North, such as Svalbard, is often not included and small Arctic settlements as typical for the Arctic are not being considered. The combination with satellite derived vegetation index (NDVI) trends allows for identification of recently build infrastructure. Our results suggest that the detectable human-impacted area in the Arctic coastal region increased by 15% since 2000. The majority can be attributed to the oil/gas industry. These findings highlight continued industrial development, which also shows up in night-time lights observations. Further developments of monitoring schemes may combine classifications with NDVI and night-time light trends. Databases on coastal dynamics currently only document coastline change (Lantuit et al 2012). Such information should be combined with information

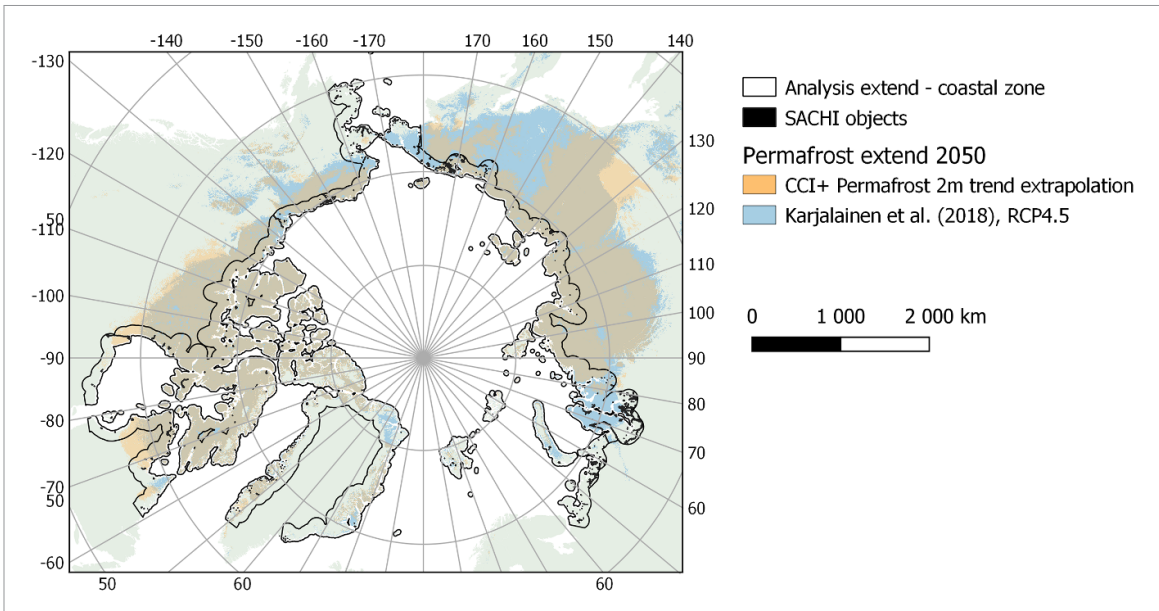


Figure 11. Distribution of Sentinel-1/2 derived human-impacted areas (SACHI objects) within the 100 km coastal zone. Background: Permafrost presence at 2 m depth (mean annual ground temperature <0 °C) in 2050 based on extrapolated trends (1997–2019; input: Obu *et al* (2021c), ground thermal modelling based on satellite derived landsurface temperature in combination with reanalyses data) and a statistical modelling result for a RCP 4.5 scenario for 2050 (source: Karjalainen *et al* 2018; mean annual ground temperature <0 °C, unspecified depth).

on settlements and built infrastructure in order to facilitate advanced vulnerability assessment at circumpolar scale.

Data availability statement

The data that support the findings of this study will be openly available following an embargo at the following URL/DOI: https://zenodo.org/record/4925911. Data will be available from 31 October 2023.

Acknowledgments

This publication is part of the Nunataryuk and CHARTER projects. The projects have received funding under the European Union's Horizon 2020 Research and Innovation Pro-

gramme under Grant Agreement Nos. 773421 and 869471. Further support was received by ESA CCI+ Permafrost, HGF AI-CORE, European Research Council project No. 885646, FFG FemTech projects CoastSAR (874213) and CoastAIMap (880182), and NSF Permafrost Discovery Gateway.

The processing scheme was developed on a highly performant virtual machine (VM) provided by the Copernicus Research and User Support (RUS). Results are based on modified Copernicus data from 2016 to 2020. The training and validation processes in this work are partially based on cadastral data of Lokalstyret in Longyearbyen, Svalbard. We also would like to acknowledge the voluntary contributors to OpenStreetMap and the anonymous reviewers for their valuable comments on the manuscript.

Appendix A. Used datasets

 Table A1. Overview of used datasets for input, comparison and evaluation.

Dataset name	Source	Туре	Used layers/ bands	Spatial coverage	Temporal coverage	Use
Sentinel-1	Copernicus Data Hub	Synthetic aperture radar	C-band, Interferometric Wide swath mode (IW), Polarizations VV/VH (most areas) or HH/HV (Greenland)	Full analyses extent, spatial resolution of 5 × 20 m	2017–2020	Input for GBM classification
Sentinel-2	Copernicus Data Hub	Multispectral	Level 1C, orthorectified images of top of atmosphere reflectance; all 10 and 20 m bands	Full analyses extent, 10 and 20 m resolution	2016–2020	Input for GBM and DL classification
Landsat	Landsat-7 and -8 archive	Multispectral	Red and Near Infrared	Full analyses extent, 30 m resolution	2000–2018	Input for NDVI trend retrieval
OpenStreetMap	Geofabrik GmbH, Karlsruhe, Germany, www.geofa brik.de/	Streets and building information in vector format	Relevant OSM objects categories: buildings, traffic, transport, railways and roads	inconsistent coverage of analyses extent	unknown	Comparison with results
Permafrost_cci	Obu <i>et al</i> (2021a, 2021b, 2021c)	Derived from a ground thermal model using landsurface temperature	Ground temperature at 2 m depth, permafrost extent, active layer thickness	Full analyses extent, 1 km resolution	1997–2019	Combination with results
Night-time lights global dataset (VNL V2)	Elvidge et al (2021)	Derived from the visible and infrared imaging suite (VIIRS) day night band (DNB) on board of JPSS satellites (joint polar-orbiting satellitesystem)	Radiances in nW cm ⁻² sr ⁻¹	Full analyses extent, 15 arc seconds resolution	2016	Combination with results
Arctic circumpolar settlements	Wang et al (2021)	Inhabited communities with known population	Point coordinates, names	Full analyses extent	2017	Comparison with results, initial input for improved settlement database
Cumulative impact map	Walker et al (2014)	Aerial photographs derived boundaries	Shapefiles with human impact as attributes	Three sites (each 20 km ²) at the Prudhoe Bay oil extraction site, US	1949–2011	Evaluation of results
Calibration data for infrastructure mapping	Lu et al (2018)	Annotated catastral information	Shapefiles of buildings and roads	Partial coverage of Longyearbyen, Svalbard	2018	Evaluation of results

Appendix B. Considered categories for use attributes

Table B1. Considered categories for use attributes at different levels. Main economic activities (use) and most relevant (general use) as well as areal extent as identified with the Sentinel-1/2 data and selected properties (average night-time light radiance in nW cm $^{-2}$ sr $^{-1}$ (NR) and normalized difference vegetation index (NDVI) trend are provided.

Use	General use	Area (km²)	NR	NDVI trend
Coal mining	Mining	4.19	No data	-0.16
Coal mining, tourism	Mining	4.51	No data	0.09
Diamonds mining	Mining	0.25	1.88	0.05
Farming	Agriculture	2.55	3.73	0.02
Fishing	Fishing	88.90	5.36	0.01
Fishing, education	Fishing	0.56	10.05	-0.02
Fishing, farming	Fishing	0.77	9.75	0.01
Fishing, gold mining	Mining	34.32	3.23	0.03
Fishing, herding	Fishing	1.91	4.39	0.04
Fishing, herding, hunting	Fishing	10.57	5.03	0.01
Fishing, hunting	Fishing	36.35	4.35	0.02
Fishing, hunting, tourism	Fishing	0.86	9.73	0.04
Fishing, tourism	Fishing	32.12	8.47	0.01
Forest	Other	1.28	1.94	0.07
Gas, herding	Gas/oil	1.00	9.84	0.01
Gas/oil	Gas/oil	410.56	31.48	-0.03
Gas/oil, tourism	Gas/oil	5.29	33.77	0.02
Gold mining	Mining	64.06	1.25	0.03
Gold & uranium mining	Mining	4.07	1.67	0.01
Herding	Agriculture	17.62	7.52	0.01
Historical	Other	1.84	1.60	0.03
Hunting	Other	2.82	0.11	0.04
Lead—zinc mining	Mining	11.22	0.00	0.02
Military	Military	39.52	3.21	0.04
Military, tourism	Military	5.12	1.80	0.01
Mining	Mining	58.20	0.48	0.04
Nature reserve	Other	0.95	7.52	-0.04
Nickel mining	Mining	51.96	3.85	-0.02
Quartz mining	Mining	0.93	0.00	0.00
Research station	Other	0.01	5.18	-0.08
Research station, coal mining	Other	0.46	No data	0.13
Tourism	Other	71.01	6.64	0.00
Transport	Other	4.83	2.46	0.03
Transport, mining	Other	16.84	2.07	0.06
Abandoned	Abandoned	32.50	0.96	0.02
Unknown	Other	67.19	2.96	0.02

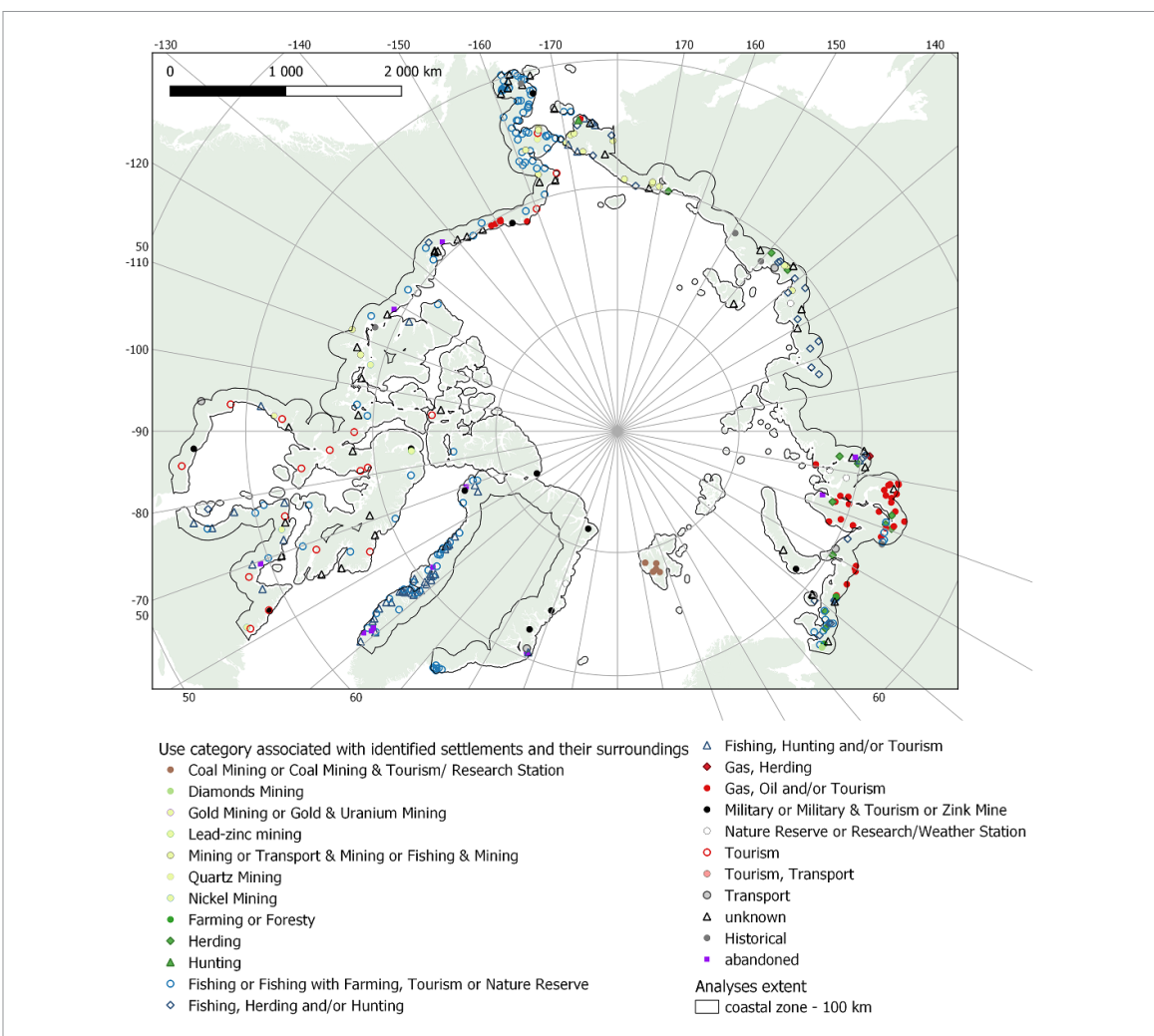


Figure B1. Assigned use categories for settlement centers with identified built infrastructure (coordinates for 285 settlements extracted from Wang *et al* (2021); 221 added using Bartsch *et al* (2021), see figure 1) based on publicly available information (analysis extent only; partially summarized, see table B1). Note, the actual extent of land use is not reflected in this representation.

Appendix C. Additional regional results plots

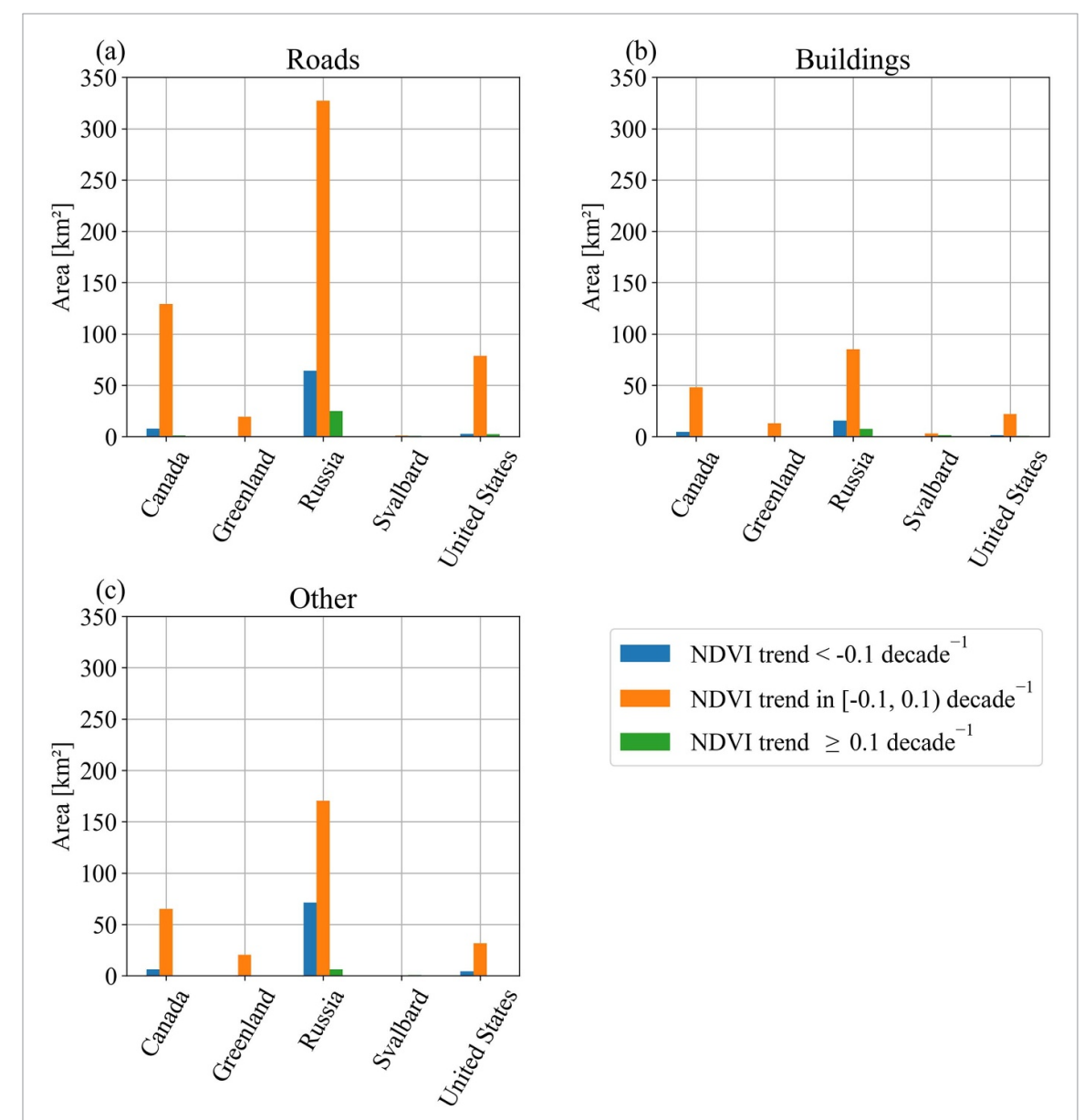


Figure C1. Area extent of Landsat-based normalized difference vegetation index (NDVI) change trends 2000–2018 for each class of human impacted areas as mapped with Sentinel-1 and -2 by country/region (analysis extent only).

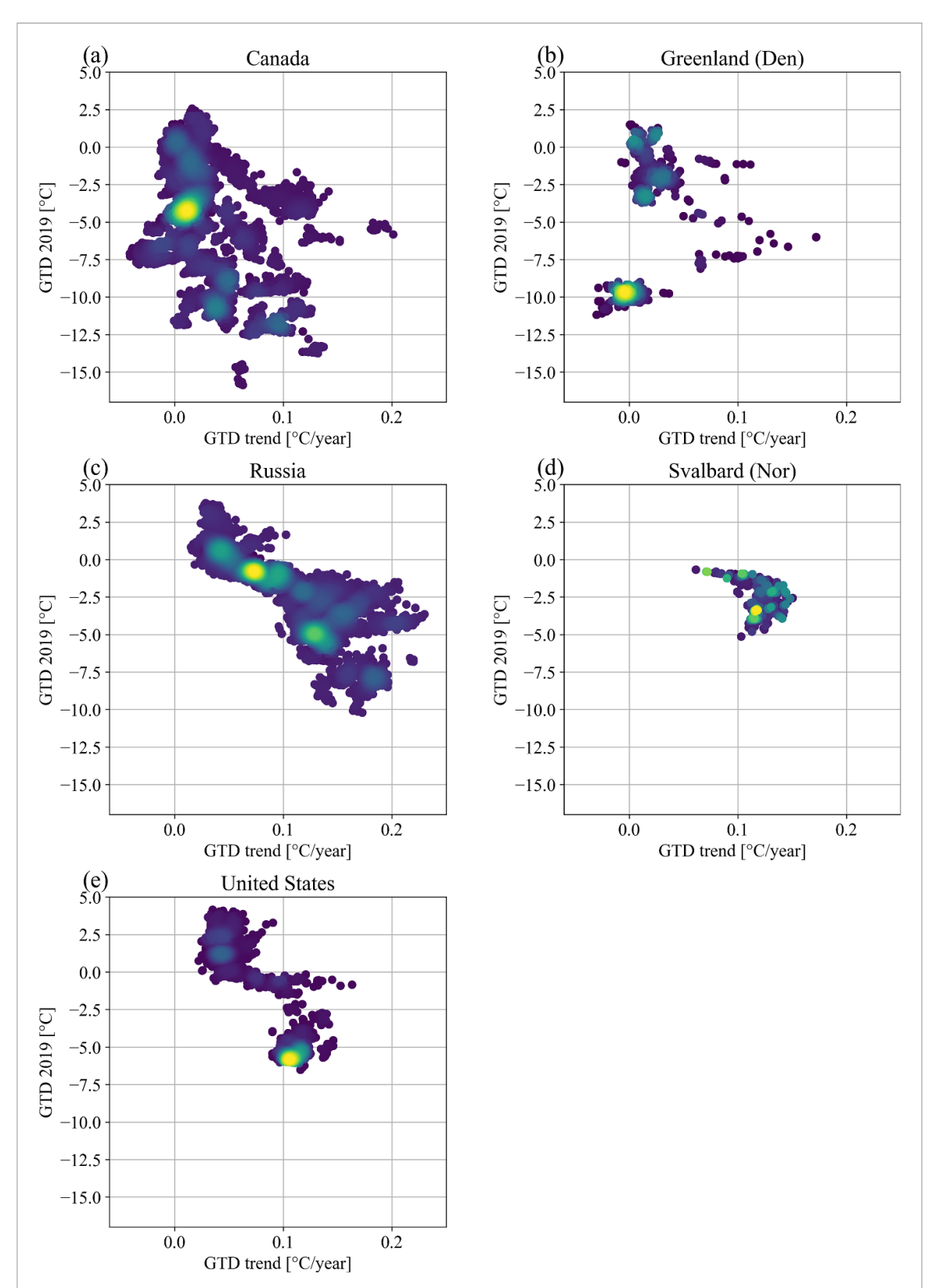


Figure C2. Scatterplots of ground temperature (GTD; 2 m depth) trend versus 2019 status for different countries/regions (analysis extent only). Each point represents the average for a distinct object (human impacted area) as mapped with Sentinel-1 and -2 (Bartsch *et al* 2021).

ORCID iDs

- Annett Bartsch https://orcid.org/0000-0002-3737-7931
- Georg Pointner https://orcid.org/0000-0003-2539-3827
- Ingmar Nitze https://orcid.org/0000-0002-1165-6852
- Guido Grosse https://orcid.org/0000-0001-5895-

References

- Adger W N, Barnett J, Chapin F S and Ellemor H 2011 This must be the place: underrepresentation of identity and meaning in climate change decision-making *Glob. Environ. Polit.* 11 1–25
- Adger W N, Dessai S, Goulden M, Hulme M, Lorenzoni I, Nelson D R, Naess L O, Wolf J and Wreford A 2009 Are there social limits to adaptation to climate change? Clim. Change 93 335–54
- Aporta C 2009 The trail as home: inuit and their pan-arctic network of routes *Hum. Ecol.* 37 131–46
- Barnhart K R, Overeem I and Anderson R S 2014 The effect of changing sea ice on the physical vulnerability of Arctic coasts *Cryosphere* 8 1777–99
- Bartsch A *et al* 2020b Feasibility of tundra vegetation height retrieval from Sentinel-1 and Sentinel-2 data *Remote Sens*. *Environ.* 237 111515
- Bartsch A, Pointner G, Ingeman-Nielsen T and Lu W 2020a Towards circumpolar mapping of Arctic settlements and infrastructure based on Sentinel-1 and Sentinel-2 *Remote Sens.* 12 2368
- Bartsch A, Pointner G and Nitze I 2021 Sentinel-1/2 derived arctic coastal human impact dataset (SACHI) *Zenodo* (available at: https://zenodo.org/record/4925911)
- Bennett M M and Smith L C 2017 Advances in using multitemporal night-time lights satellite imagery to detect, estimate and monitor socioeconomic dynamics *Remote Sens. Environ.* **192** 176–97
- Biskaborn B K et~al~2019 Permafrost is warming at a global scale $\it Nat.~Commun.~10~1-11$
- Box J E et al 2019 Key indicators of Arctic climate change: 1971–2017 Environ. Res. Lett. 14 045010
- Brady M B and Leichenko R 2020 The impacts of coastal erosion on Alaska's North slope communities: a co-production assessment of land use damages and risks *Polar Geogr.* 43 259–79
- Chen T and Guestrin C 2016 XGBoost: a scalable tree boosting system *Proc. 22nd ACM SIGKDD Int. Conf. Knowledge Discovery and Data Mining—KDD'16* (ACM Press)
- Chollet F 2017 Deep Learning With Python (Shelter Island, NY: Manning)
- Ehrich D, Thuestad A E, Tømmervik H, Fauchald P and Hausner V H 2018 Local land use associated with socio-economic development in six arctic regions *Ambio* 48 649–60
- Elvidge C D, Baugh K, Zhizhin M, Hsu F C and Ghosh T 2017 VIIRS night-time lights *Int. J. Remote Sens.*
- Elvidge C D, Zhizhin M, Ghosh T, Hsu F-C and Taneja J 2021 Annual time series of global VIIRS nighttime lights derived from monthly averages: 2012 to 2019 *Remote Sens*. 13 922
- Ford J D, McDowell G and Pearce T 2015 The adaptation challenge in the Arctic Nat. Clim. Change 5 1046–53
- Fritz M, Vonk J E and Lantuit H 2017 Collapsing Arctic coastlines Nat. Clim. Change 7 6–7

- Georganos S, Grippa T, Vanhuysse S, Lennert M, Shimoni M and Wolff E 2018 Very high resolution object-based land use–land cover urban classification using extreme gradient boosting *IEEE Geosci. Remote Sens. Lett.* **15** 607–11
- Hjort J, Karjalainen O, Aalto J, Westermann S, Romanovsky V E, Nelson F E, Etzelmüller B and Luoto M 2018 Degrading permafrost puts arctic infrastructure at risk by mid-century Nat. Commun. 9 5147
- IPCC 2021 Climate Change 2021: The Physical Science Basis. Contribution of Working Group I to the Sixth Assessment Report of the Intergovernmental Panel on Climate Change (Cambridge: Cambridge University Press)
- IPCC 2019 IPCC Special Report on the Ocean and Cryosphere in a Changing Climate Pörtner HO, Roberts DC, Masson-Delmotte V, Zhai P, Tignor M, Poloczanska E, Mintenbeck K, Alegria A, Nicolai M, Okem A, Petzold J, Rama B and Weyer N M (www.ipcc.ch/srocc/cite-report)
- Irrgang A M, Lantuit H, Gordon R R, Piskor A and Manson G K 2019 Impacts of past and future coastal changes on the Yukon coast—threats for cultural sites, infrastructure and travel routes *Arct. Sci.* 5 107–26
- Jordahl K et al 2021 geopandas/geopandas: v0.8.2 Zenodo (available at: https://doi.org/10.5281/zenodo.4464949)
- Karjalainen O, Aalto J, Luoto M, Westermann S, Romanovsky V E, Nelson F E, Etzelmüller B and Hjort J 2018 Circumpolar raster grids of permafrost extent and geohazard potential for near-future climate scenarios PANGAEA (available at: https://doi.pangaea.de/10.1594/PANGAEA.893881)
- Kumpula T, Forbes B C, Stammler F and Meschtyb N 2012 Dynamics of a coupled system: multi-resolution remote sensing in assessing social-ecological responses during 25 years of gas field development in Arctic Russia *Remote Sens*. 4 1046–68
- Lantuit H *et al* 2012 The Arctic coastal dynamics database: a new classification scheme and statistics on Arctic permafrost coastlines *Estuaries Coasts* 35 383–400
- Larsen J N *et al* 2021 Thawing permafrost in Arctic coastal communities: a framework for studying risks from climate change *Sustainability* **13** 2651
- Lu W, Aalberg A, Høyland K, Lubbad R, Løset S and Ingeman-Nielsen T 2018 Calibration data for infratructure mapping in Svalbard, link to files *PANGAEA* (available at: https://doi.pangaea.de/10.1594/PANGAEA.895950)
- Nitze I and Grosse G 2016 Detection of landscape dynamics in the Arctic lena delta with temporally dense landsat time-series stacks *Remote Sens. Environ.* **181** 27–41
- Nitze I, Grosse G, Jones B M, Romanovsky V E and Boike J 2018 Remote sensing quantifies widespread abundance of permafrost region disturbances across the Arctic and subarctic Nat. Commun. 9 5423
- O'Brien K L and Leichenko R M 2000 Double exposure: assessing the impacts of climate change within the context of economic globalization *Glob. Environ. Change* 10 221–32
- O'Garra T 2017 Economic value of ecosystem services, minerals and oil in a melting Arctic: a preliminary assessment *Ecosyst.* Serv. 24 180–6
- Obu J et al 2021a ESA permafrost climate change initiative (permafrost_cci): permafrost active layer thickness for the northern hemisphere, v3.0', CEDA (available at: https://catalogue.ceda.ac.uk/uuid/67a3f8c8dc914ef99 f7f08eb0d997e23)
- Obu J et al 2021b ESA permafrost climate change initiative (permafrost_cci): permafrost extent for the northern hemisphere, v3.0', CEDA (available at: https://catalogue.ceda.ac.uk/uuid/6e2091cb0c8b4106921b63cd5357c97c)
- Obu J et al 2021c ESA permafrost climate change initiative (permafrost_cci): permafrost ground temperature for the northern hemisphere, v3.0', CEDA (available at: https://catalogue.ceda.ac.uk/uuid/b25d4a6174de4ac 78000d034f500a268)
- Preston B L, Yuen E J and Westaway R M 2011 Putting vulnerability to climate change on the map: a review

- of approaches, benefits and risks *Sustain. Sci.* **6** 177–202
- Ramage J, Jungsberg L, Wang S, Westermann S, Lantuit H and Heleniak T 2021 Population living on permafrost in the Arctic *Popul. Environ.* **43** 22–38
- Ramm F 2019 OpenStreetMap Data in Layered GIS Format, Free Shapefiles—2019-11-06 (available at: http://download. geofabrik.de/osm-data-in-gis-formats-free.pdf)
- Ramm F 2020 OpenStreetMap Data in Layered GIS Format, Version 0.7.9 (Geofabrik)
- Raynolds M K *et al* 2014 Cumulative geoecological effects of 62 years of infrastructure and climate change in ice-rich permafrost landscapes, Prudhoe Bay Oilfield, Alaska *Glob. Change Biol.* 20 1211–24
- Romanovsky V *et al* 2017 Changing permafrost and its impacts *Snow, Water, Ice and Permafrost in the Arctic (Swipa)* (Oslo, Norway: Arctic Monitoring and Assessment Programme (AMAP)) pp 65–102
- Sen P K 1968 Estimates of the regression coefficient based on Kendall's tau J. Am. Stat. Assoc. 63 1379–89

- Suter L, Streletskiy D and Shiklomanov N 2019 Assessment of the cost of climate change impacts on critical infrastructure in the circumpolar Arctic *Polar Geogr.* 42 267–86
- Theil H 1992 A rank-invariant method of linear and polynomial regression analysis *Henri Theil's Contributions to Economics* and Econometrics Raj B and Koerts J (Dordrecht: Springer Netherlands) pp 345–81
- Walker D A, Raynolds M K, Buchhorn M and Peirce J L 2014 Landscape and permafrost changes in the Prudhoe Bay Oilfield, Alaska *Alaska Geobotany Center Publication AGC* 14-01 (available at: http://arcticatlas.geobotany.org/catalog/ entries/5470-prudhoe-bay-cumulative-impact-map-araynolds-2014)
- Wang S, Ramage J, Bartsch A and Efimova A 2021 Population in the Arctic circumpolar permafrost region at settlement level *Zenodo* (available at: https://doi.org/10.5281/ ZENODO.4529610)
- Westermann S, Østby T I, Gisnås K, Schuler T V and Etzelmüller B 2015 A ground temperature map of the North Atlantic permafrost region based on remote sensing and reanalysis data *Cryosphere* 9 1303–19